






An integrated wavemeter based on fully-stabilized resonant electro-optic frequency comb

Rui Niu^{1,2,3,6}, Shuai Wan^{1,2,3,6}, Wenjian Li⁴, Pi-Yu Wang^{1,2,3}, Fang-Wen Sun^{1,2,3} , Fang Bo⁴ , Junqiu Liu^{3,5} , Guang-Can Guo^{1,2,3} & Chun-Hua Dong^{1,2,3}  

Optical frequency combs provide a powerful tool for precise measurement of the optical frequency, holding significant importance in fields such as spectroscopy, optical communication and optical clock. The frequency stability of the comb line determines the precision of the frequency measurement, but the delicate interplay between high precision, low power consumption and integration still needs to be optimized. To this aim, here we demonstrate a frequency measurement scheme based on a fully stabilized electro-optic comb, in which the pump laser frequency and repetition rate are independently locked to the atomic transition and microwave signal. The measurement precision of the demonstrated wavemeter can reach sub-kHz-level, and the parallel measurement of multiple wavelengths can be performed. Therefore, by combining the technical scheme reported here with advanced integrated functional devices, our system is expected to provide a feasible solution for chip-scale frequency precision measurement and reference.

¹CAS Key Laboratory of Quantum Information, University of Science and Technology of China, Hefei, Anhui 230026, People's Republic of China. ²CAS Center For Excellence in Quantum Information and Quantum Physics, University of Science and Technology of China, Hefei, Anhui 230088, People's Republic of China. ³Hefei National Laboratory, University of Science and Technology of China, Hefei, Anhui 230088, People's Republic of China. ⁴MOE Key Laboratory of Weak-Light Nonlinear Photonics, TEDA Applied Physics Institute and School of Physics, Nankai University, Tianjin 300457, People's Republic of China. ⁵International Quantum Academy, 518048 Shenzhen, People's Republic of China. ⁶These authors contributed equally: Rui Niu, Shuai Wan. email: bofang@nankai.edu.cn; chunhua@ustc.edu.cn

Determination of laser frequency with high resolution is important in spectroscopy, metrology, and communications^{1–7}. Traditionally, measurements have been conducted using grating and interferometer-based spectrometers, but more recently these measurements have been made using optical frequency combs (OFCs)^{8,9}. However, traditional platforms based on fiber combs are bulky with a small repetition rate. When measuring frequency, the uncertainty of the repetition rate is amplified N times and transferred to the uncertainty of the frequency measurement, where N is the relative mode number of the closest comb line to the measured signal^{10,11}. Therefore, the most direct way to reduce frequency measurement uncertainty is to employ the OFC with a higher repetition frequency.

In recent years, advancements in microfabrication technology have enabled precise dispersion engineering and ultra-low propagation loss, leading to the rapid development of integrated dissipative Kerr solitons (DKSs)^{10,12–18}. Compared to traditional fiber combs, DKSs have a repetition rate that is increased by hundreds or thousands of times, which can effectively reduce the uncertainty of frequency measurement^{19,20}. However, a fully frequency-stabilized DKS requires the stabilization of the repetition rate (f_{rep}) as well as one of the carrier-envelope-offset frequencies (f_{ceo}) and the pump frequency (f_p) because of $f_p = nf_{\text{rep}} + f_{\text{ceo}}$. Due to the intracavity complex nonlinear dynamics, stabilizing these parameters is challenging, as they are interdependent and coupled together²¹. To stabilize these key parameters, precise control over the pump laser power, pump laser frequency, and laser-cavity detuning is required to achieve frequency stabilization. This typically involves the use of auxiliary fiber comb systems and multiple locking loops, significantly increasing the difficulty and complexity of the system integration^{2,3,22}.

In addition to DKSs, another approach for generating on-chip OFCs that relies on the electro-optic (EO) modulation has recently emerged^{23–28}. The repetition rate of the EO comb is uniquely defined by the modulation frequency. Conventionally, EO combs are generated by modulating continuous light with a series of discrete phase and amplitude modulators²⁹. Since light passes through each modulator only once, the EO modulation strength is relatively weak and the span of the generated EO comb is typically only a few nanometers^{30,31}. Benefiting from recent technological advancements in the lithium niobate on insulator (LNOI) platform^{32–39}, the light in the high-quality factor (Q) on-chip lithium niobate (LN) microresonators can circulate and pass through the EO modulation area multiple times, resulting in a significant improvement in the modulation strength. The

cascaded sideband generation process effectively generates numerous comb lines with modulation frequency intervals, significantly expanding the span of the EO comb. Moreover, the generation of the EO comb does not need a pump threshold, complex trigger, or stabilization schemes, considerably reducing the requirements on the pump laser source and control equipment. Thus, EO combs offer a compelling alternative for chip-scale frequency precision measurement.

Here, we demonstrate a high-precision on-chip wavemeter based on the LNOI platform. The repetition rate of the EO comb is around 19.5 GHz with a comb spanning approximately 40 nm. The pump laser around 1560 nm is stabilized by the atomic transition of ⁸⁷Rb with the help of the periodically poled lithium niobate (PPLN) waveguide⁴⁰. On the basis of this fully stabilized EO comb, the frequency precision of the wavemeter is obtained at about sub-kHz. This represents an improvement of three orders of magnitude compared to prior work employing the dual-comb technique¹⁹. In addition, we measure the wavelengths of four lasers simultaneously, demonstrating the ability to measure multiple wavelengths in parallel. Our work indicates that the wavemeter based on EO comb has the potential to far exceed that of commercial tabletop wavemeters, providing a competitive pathway towards future chip-scale frequency precision measurement.

Results

Schematic and device fabrication. The schematic of the high-precision wavemeter is illustrated in Fig. 1a. The pump laser is coupled into the microring resonator and generates the EO comb when the driven radio frequency (RF) matches the free spectral range (FSR) of the microring. As shown in Fig. 1b, the frequency of the comb lines can be expressed as $f_\mu = f_p + \mu f_{\text{rep}}$, where μ is the relative mode number with respect to the pump resonance mode. f_{rep} is the repetition rate and referenced by the rubidium maser-referenced frequency, and f_p is the frequency of the pump laser and stabilized by the atomic transition. Here, f_μ can be fully determined and used as a reliable frequency reference. When the target laser is combined with the stabilized EO comb, the beating signal Δf is obtained and the frequency of the target laser can be expressed as $f_m = f_p + \mu f_{\text{rep}} \pm \Delta f - \Omega$, where the Ω is the modulation frequency of the acousto-optic modulator (AOM). Therefore, a shift of the f_{rep} induces a shift in the Δf by a factor of μ . We can obtain the absolute value of μ , as $|\mu| = |\partial \Delta f / \partial f_{\text{rep}}|$ by measuring the shift of Δf with varying the f_{rep} . With changing the

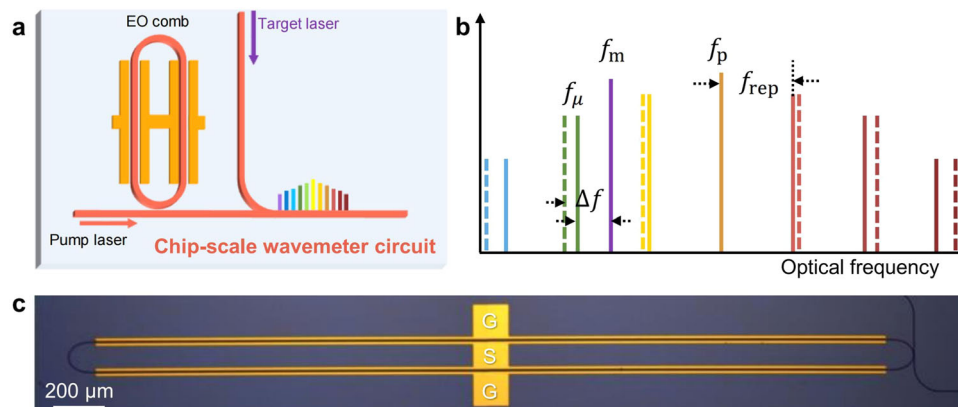


Fig. 1 The schematic and operating principle of the wavemeter. **a** The schematic of the chip-scale wavemeter circuit. The electro-optic (EO) comb is generated in a lithium niobate (LN) resonator using the stabilized pump laser. The target laser is combined with the stabilized EO comb to validate the performance of the EO comb for frequency measurement. **b** The operating principle of the wavemeter. Through detecting the beat frequency (Δf) between the target laser and the adjacent comb line and analyzing the relative mode number μ of the adjacent comb line and the sign before the Δf , the frequency of the target laser $f_m = f_p + \mu f_{\text{rep}} \pm \Delta f$ can be obtained. **c** Optical micrograph of the LN microring resonator. S(G) denotes the signal (ground) electrode.

modulation frequency of AOM, f_m is decreased in our experiment. Then, the sign before Δf and the relative mode number μ can be deduced by the drift of the beating signal, leading to the determination of the f_m ²⁰. If the Δf increases with the decrease of the f_m , the sign before Δf is negative. Otherwise, the sign before Δf is positive. Furthermore, if the sign before Δf is different from the sign of $\partial\Delta f/\partial f_{\text{rep}}$, the sign of μ is positive. On the contrary, the sign of μ is negative.

The device employed for generating EO combs is fabricated from a commercial x-cut 600-nm LNOI wafer (NANOLN). The wafer is made up of 600-nm-thick x-cut LN, 2- μm -thick wet oxidation silicon dioxide (SiO_2), and 500- μm -thick silicon. Electron-beam lithography is used to pattern the device with hydrogen-silsesquioxane (HSQ) resist. Following the development of the pattern, the LN film is partially etched by argon-ion-based reactive ion etching in an inductively coupled plasma (ICP) etcher to form a 330-nm-depth trapezoidal waveguide cross-section with a remaining slab of 270 nm. The device is then cleaned by buffered HF solution and RCA1 cleaning solution. The microwave electrodes are patterned using laser direct writing and the metal (15 nm of chromium, 300 nm of gold) is transferred using thermal evaporation and the bilayer lift-off process. Finally, the facet of the chip was diced to enable good fiber-to-chip light coupling. The optical micrograph of our device is shown in Fig. 1c. The air-cladded LN microring resonator with a top width of 1.4 μm and a sidewall angle of around 60° has an FSR of around 19.5 GHz. The fiber-to-chip coupling loss in the communication band is approximately 6 dB per facet.

Experimental setup and EO comb characterization. We carry out the experiments with the setup shown in Fig. 2a. A portion of the pump laser (Toptica CTL 1550) is frequency-doubled through the PPLN and passes through the atomic gas cell to obtain the saturation absorption spectrum. Then, the frequency-doubled laser is locked to the atomic transition line through the Pound–Drever–Hall (PDH) locking⁴¹. When the pump laser is stabilized, one fundamental TE mode around 1560.48 nm in the LN cavity is tuned by external temperature control to match the frequency of the locked pump laser. The linewidth of the resonance mode used in the experiment is approximately 149 MHz, corresponding to a loaded Q of 1.29×10^6 . An RF signal around 19.503 GHz, matching the FSR of the microresonator, is used to drive the microwave electrode. The EO comb is generated with the spans of 40 nm from 1540 to 1580 nm, as shown in Fig. 2b. The on-chip pump power is 2 mW and the RF driven power is 33 dBm, respectively. Figure 2c illustrates the electrical spectrum

of the detected 19.503 GHz RF signal, corresponding to the repetition rate of the EO comb. By tuning the modulation frequency of the RF signal and recording the corresponding repetition rate, it can be seen that the repetition rate and the modulation frequency are exactly the same, as shown in Fig. 2d, which indicates that the repetition rate is fully determined by the RF modulation signal^{23,24}.

Stability characterization. To characterize the frequency stability of the fully stabilized EO comb, we further test the Allan deviation of the repetition rate, the pump laser, and the comb line. As shown in Fig. 3a, due to the excellent stability provided by the

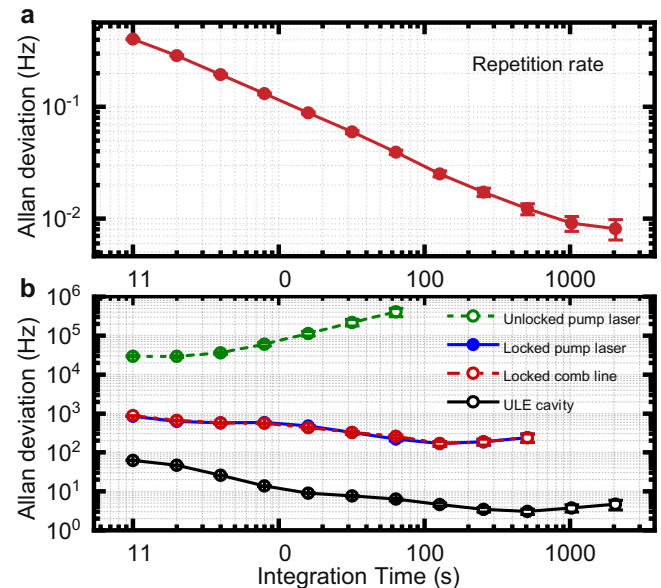


Fig. 3 Performance of the wavemeter. a The Allan deviation of the repetition rate of the EO comb. The frequency stability of the repetition rate reaches 0.4 Hz at 1 s of measurement time. **b** The Allan deviation of the pump laser frequency for unlocked (hollow green circles) and locked state (solid blue circles). At a measurement time of 1 s, the frequency stability is improved from 30 kHz to 0.9 kHz. The Allan deviation of one comb line ($\mu = 50$) (hollow red circles) and the ULE cavity-referenced laser (hollow black circles). At a measurement time of 1 s, the frequency stability of the locked comb line reaches 0.9 kHz, and the stability reaches 0.2 kHz at 512 s of measurement time, indicating a sub-kHz-level frequency measurement precision. Error bars represent a 68% confidence interval.

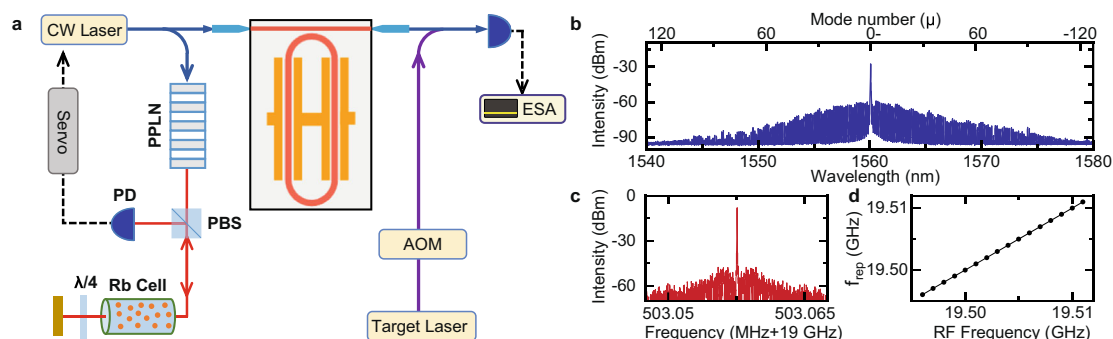


Fig. 2 Experimental setup and electro-optic (EO) comb performance. a Schematic of the experimental setup. The pump laser frequency is locked to the atomic transition line of ^{87}Rb via a periodically poled lithium niobate (PPLN) frequency doubler. The driving RF signal of the EO comb comes from a rubidium-clock-referenced RF source. PBS: polarization beam splitter, AOM: acousto-optic modulator, PD: photodetector, ESA: electronic spectrum analyzer. **b** The typical optical spectrum of the EO comb. The on-chip pump power is 2 mW and the driven RF power is 33 dBm. **c** The electrical spectrum with a microwave signal of 19.503 GHz, corresponds to the repetition rate of the EO comb. **d** Measured repetition rate versus the modulation frequency. The two frequencies are identical, indicating that the repetition rate is completely determined by the modulation frequency.

rubidium clock, the frequency stability of the repetition rate reaches 0.4 Hz at 1 s of measurement time. Moreover, the stability improves over the long term, which can reach 9 mHz at 1024 s of measurement time. To characterize the stability of the pump laser, we introduce another laser that is referenced to the same atomic transition of ^{87}Rb through another rubidium cell. The Allan deviation of the single laser can be obtained by dividing the Allan deviation of the beat frequency of these two lasers by $\sqrt{2}$. Figure 3b shows the frequency stability of the pump laser, which is also significantly improved after locking to the atomic transition. The stability at 1 s of measurement time is improved from 30 kHz in the unlocked (free-running) state to 0.9 kHz in the locked state, which is about three orders of magnitude higher than the repetition rate. Therefore, the frequency stability of the comb lines is mainly determined by the frequency stability of the pump laser³, where maximal $|\mu|$ is only around 120 in our experiment.

To obtain the Allan deviation of the comb line, we introduce a reference laser that is referenced to a reference cavity with a finesse of 1000 and a linewidth of 1.5 MHz. The Allan deviation of the comb line (hollow red circles in Fig. 3b) is obtained by measuring the Allan deviation of the beat frequency between the comb line ($\mu = 50$) and the reference laser, where removing the Allan deviation of the reference laser (hollow black circles in Fig. 3b). It can be seen that the Allan deviation of the comb line is nearly identical to that of the pump laser, and the effect of the Allan deviation of the repetition rate is extremely small. Therefore, the Allan deviation for other comb lines could be deduced with a similar level, indicating a kHz-level frequency measurement precision (0.9 kHz at 1 s measurement time). For longer measurement time, the stability can reach 0.2 kHz at 512 s of measurement time, and the corresponding measurement precision could reach the sub-kHz level.

Operation of wavemeter. To demonstrate the operation process and performance of the high-precision wavemeter, we launch four target lasers and simultaneously measure their wavelengths based on this fully stabilized EO comb. These target lasers are locked to the reference cavity (finesse of 1000 and linewidth of 1.5 MHz). One target laser operates at around 1552 nm, and the other three target lasers are the modulated lasers including two sidebands, which are generated by the electro-optic phase modulator laser and around 1564 nm. These target lasers are combined with the fiber beam splitter and mixed with the fully stabilized EO comb for wavelength measurement. The beating signal between the comb line and the target laser is detected using a photodetector with a bandwidth of 12.5 GHz and recorded on the real-time spectrum analyzer (Rohde & Schwarz, FSVR). Figure 4 shows the real-time evolution of the beat note between the four probe lasers and the adjacent comb lines over a 20-s period. Initially, the modulation frequency of the AOM is switched from

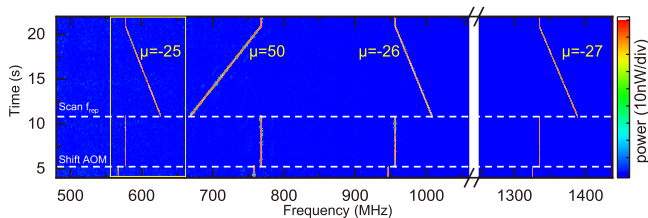


Fig. 4 Demonstration of the multi-wavelength measurements. Real-time evolution of the beat frequency between target lasers and the comb lines during the operation of the wavemeter. Firstly, the modulation frequency of the AOM is switched from 100 MHz to 90 MHz. Then, f_{rep} is tuned from 19.5005 GHz to 19.5025 GHz within 10 s.

100 MHz to 90 MHz, causing Δf to shift accordingly. Subsequently, the repetition rate f_{rep} is gradually tuned from 19.5005 GHz to 19.5025 GHz, spanning 2 MHz. As indicated in the box in Fig. 4, the Δf changes by -49.95 MHz when varying the repetition rate, corresponding to the slope -49.95 MHz/2 MHz = -24.98 . Therefore, the absolute value of integer μ can be determined as $|\mu| = 25$. Based on the behavior of Δf , we can deduce that the sign before Δf is negative and $\mu = -25$ as mentioned before. Consequently, the accurate frequency of this target laser can be determined by the atomic transition, the μ , f_{rep} , and Δf . For other target lasers shown in Fig. 4, we can determine their accurate frequency by the same analysis process. The accuracy of the wavemeter depends on the atomic transition, which is obtained at about 1 kHz at 1 s as mentioned before. The demonstrated high-precision wavemeter enables the parallel measurement of multiple wavelengths.

Conclusions

In conclusion, we successfully demonstrate an on-chip wavemeter with frequency measurement precision at sub-kHz level. Due to the generation mechanism of the EO comb, the pump laser frequency and repetition rate can be stabilized by locking to atomic transition after frequency doubling and driving the electrodes with an atomic-referenced RF source, respectively. This eliminates the need for the additional reference laser and $f-2f$ self-reference technique for the system, providing a considerable simplification in technology and equipment. Simultaneous multi-wavelength measurement holds significant applicative value in fields such as real-time spectral analysis and high-capacity optical communication testing. It serves to mitigate the inherent asynchrony associated with time-division measurements in spectroscopy and enables rapid and precise measurement of multi-channel wavelengths. The fully stabilized EO comb-based system permits the parallel measurement of multiple wavelengths and has a measurement precision that can reach a sub-kHz level with sufficient integration time.

Here, the measurement precision of the system is mainly limited by the frequency stability of the pump laser. To improve the performance of the system, it can be further optimized the frequency stability of the pump laser, for example, locking the pump laser to both the atomic transition and the reference cavity⁴². Moreover, the span and the conversion efficiency of the EO comb can also be improved by increasing the Q of the microresonator and using a coupled-resonator structure^{25,32}. Particularly, the microresonator-based DKSSs offer a broader bandwidth^{43,44}. Combining the respective advantages of the DKSSs and EO combs, the wavelength detection range of the wavemeter can be greatly broadened. Additionally, components within our system, such as frequency doublers and shifters, also hold promise for integration^{3,15,45-49}. These foreseeable developments provide a promising avenue for compact, low-cost, and broadband frequency precision measurements.

Methods

Stabilization and calibration. The frequency of the comb line is determined by $f_{\mu} = f_p + \mu f_{\text{rep}}$, which means that the stabilization of the EO comb involves the stabilizing frequency of the pump laser and the repetition rate. We have employed a PDH frequency stabilization technique to lock the frequency of the pump laser (Toptica CTL 1550) to the D_2 transition of ^{87}Rb ($f_{\text{atom}} = 384.2281152033(77)$ THz)⁵⁰. The Rb cell used is a pure cell, and its temperature is set to room temperature. The frequency of the pump laser is doubled through the PPLN waveguide, and the temperature of the PPLN is controlled using a proportion-integral-derivative (PID) servo. The doubled pump

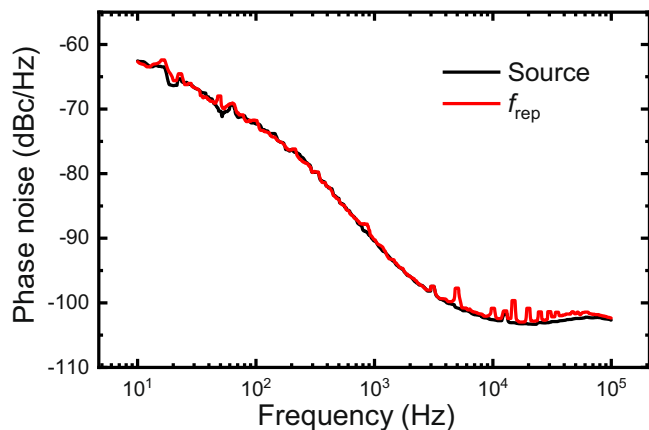


Fig. 5 Phase noise measurement of the repetition rate and the RF source.

The phase noise of the RF source (black curve) and the repetition rate (red curve) are at the same level.

laser frequency is accurately referenced to the atomic transition by providing feedback to control the current and PZT voltage of the pump laser. Then, we can get the $f_p = f_{\text{atom}}/2 = 192.1140576017(39)$ THz.

The repetition rate of the EO comb is uniquely determined by the RF signal (Rohde and Schwarz, SMB 100A), which is synchronized with the rubidium clock and amplified using a microwave amplifier. The absolute frequency of the target laser is calculated using $f_m = f_p + \mu f_{\text{rep}} \pm \Delta f - \Omega$, where f_{rep} is defined by the RF signal, and Δf is measured using a real-time spectrum analyzer (Rohde & Schwarz, FSVR), which is synchronized with the same rubidium clock. To verify the relationship between the RF signal and f_{rep} , we have respectively measured their phase noise using a phase noise analyzer (Rohde & Schwarz, FSWP). The results are shown in Fig. 5, confirming that the phase noise of the RF signal and the repetition rate are at the same level. Based on the $\mu = -25$ and the negative Δf , we deduce that the absolute frequency of one target laser is 191.6258278847(39) THz. Other frequencies of the target lasers can be calibrated as the same methods.

Data availability

All data generated or analyzed during this study are available within the paper. Further source data will be made available on request.

Code availability

The code and the algorithm used in this study are available from the corresponding author upon reasonable request.

Received: 30 July 2023; Accepted: 7 November 2023;

Published online: 16 November 2023

References

- Yu, M. et al. Silicon-chip-based mid-infrared dual-comb spectroscopy. *Nat. Commun.* **9**, 1869 (2018).
- Stern, L. et al. Direct Kerr frequency comb atomic spectroscopy and stabilization. *Sci. Adv.* **6**, eaax6230 (2020).
- Newman, Z. L. et al. Architecture for the photonic integration of an optical atomic clock. *Optica* **6**, 680 (2019).
- Drake, T. E. et al. Terahertz-rate Kerr-microresonator optical clockwork. *Phys. Rev. X* **9**, 031023 (2019).
- Marin-Palomo, P. et al. Microresonator-based solitons for massively parallel coherent optical communications. *Nature* **546**, 274 (2017).
- Corcoran, B. et al. Ultra-dense optical data transmission over standard fibre with a single chip source. *Nat. Commun.* **11**, 2568 (2020).
- Jørgensen, A. A. et al. Petabit-per-second data transmission using a chip-scale microcomb ring resonator source. *Nat. Photonics* **16**, 798 (2022).
- Udem, T., Holzwarth, R. & Hänsch, T. W. Optical frequency metrology. *Nature* **416**, 233 (2002).
- Diddams, S. A., Bergquist, J. C., Jefferts, S. R. & Oates, C. W. Standards of time and frequency at the outset of the 21st century. *Science* **306**, 1318 (2004).
- Diddams, S. A., Vahala, K. & Udem, T. Optical frequency combs: coherently uniting the electromagnetic spectrum. *Science* **369**, eaay3676 (2020).
- Nishimoto, K., Minoshima, K., Yasui, T. & Kuse, N. Investigation of the phase noise of a microresonator soliton comb. *Optics Express* **28**, 19295 (2020).
- Kippenberg, T. J., Gaeta, A. L., Lipson, M. & Gorodetsky, M. L. Dissipative Kerr solitons in optical microresonators. *Science* **361**, eaan8083 (2018).
- Liu, J. et al. Emerging material platforms for integrated microcavity photonics. *Sci. China Phys. Mechan. Astron.* **65**, 104201 (2022).
- Shen, B. et al. Integrated turnkey soliton microcombs. *Nature* **582**, 365 (2020).
- Xiang, C. et al. Laser soliton microcombs heterogeneously integrated on silicon. *Science* **373**, 99 (2021).
- Nie, M. et al. Dissipative soliton generation and real-time dynamics in microresonator-filtered fiber lasers. *Light* **11**, 296 (2022).
- Lu, Z. et al. Synthesized soliton crystals. *Nat. Commun.* **12**, 3179 (2021).
- Wang, C. et al. Soliton formation and spectral translation into visible on CMOS-compatible 4h-silicon-carbide-on-insulator platform. *Light* **11**, 341 (2022).
- Yang, Q.-F. et al. Vernier spectrometer using counterpropagating soliton microcombs. *Science* **363**, 965 (2019).
- Niu, R. et al. kHz-precision wavemeter based on reconfigurable microsoliton. *Nat. Commun.* **14**, 1 (2023).
- Stone, J. R. et al. Thermal and nonlinear dissipative-soliton dynamics in Kerr-microresonator frequency combs. *Phys. Rev. Lett.* **121**, 063902 (2018).
- Spencer, D. T. et al. An optical-frequency synthesizer using integrated photonics. *Nature* **557**, 81 (2018).
- Zhang, M. et al. Broadband electro-optic frequency comb generation in a lithium niobate microring resonator. *Nature* **568**, 373 (2019).
- Rueda, A., Sedlmeir, F., Kumari, M., Leuchs, G. & Schwefel, H. G. L. Resonant electro-optic frequency comb. *Nature* **568**, 378 (2019).
- Hu, Y. et al. High-efficiency and broadband on-chip electro-optic frequency comb generators. *Nat. Photonics* **16**, 679 (2022).
- Yu, M. et al. Integrated femtosecond pulse generator on thin-film lithium niobate. *Nature* **612**, 252 (2022).
- Zhu, D. et al. Spectral control of nonclassical light pulses using an integrated thin-film lithium niobate modulator. *Light* **11**, 327 (2022).
- Zhang, K. et al. A power-efficient integrated lithium niobate electro-optic comb generator. *Commun. Phys.* **6**, 17 (2023).
- Metcalf, A. J., Torres-Company, V., Leaird, D. E. & Weiner, A. M. High-power broadly tunable electrooptic frequency comb generator. *IEEE J. Select. Top. Quantum Electron.* **19**, 231 (2013).
- Sakamoto, T., Kawanishi, T. & Izutsu, M. Asymptotic formalism for ultraflat optical frequency comb generation using a Mach-Zehnder modulator. *Opt. Lett.* **32**, 1515 (2007).
- Ozharar, S., Quinlan, F., Ozdur, I., Gee, S. & Delfyett, P. J. Ultraflat optical comb generation by phase-only modulation of continuous-wave light. *IEEE Photonics Technol. Lett.* **20**, 36 (2008).
- Liang, H., Luo, R., He, Y., Jiang, H. & Lin, Q. High-quality lithium niobate photonic crystal nanocavities. *Optica* **4**, 1251 (2017).
- He, Y. et al. Self-starting bi-chromatic LiNbO₃ soliton microcomb. *Optica* **6**, 1138 (2019).
- Hu, Y., Reimer, C., Shams-Ansari, A., Zhang, M. & Lončar, M. Realization of high-dimensional frequency crystals in electro-optic microcombs. *Optica* **7**, 1189 (2020).
- Gong, Z., Liu, X., Xu, Y. & Tang, H. X. Near-octave lithium niobate soliton microcomb. *Optica* **7**, 1275 (2020).
- Bao, C. et al. Architecture for microcomb-based GHz-mid-infrared dual-comb spectroscopy. *Nat. Commun.* **12**, 6573 (2021).
- Shams-Ansari, A. et al. Thin-film lithium-niobate electro-optic platform for spectrally tailored dual-comb spectroscopy. *Commun. Phys.* **5**, 88 (2022).
- Javid, U. A. et al. Chip-scale simulations in a quantum-correlated synthetic space. *Nat. Photonics* **17**, 883–890 (2023).
- Hwang, A. Y. et al. Mid-infrared spectroscopy with a broadly tunable thin-film lithium niobate optical parametric oscillator. Preprint at *arXiv* <https://doi.org/10.48550/arXiv.2307.04199> (2023).
- Xie, J. et al. Infrared laser locking to a rubidium saturated absorption spectrum via a photonic chip frequency doubler. *Opt. Lett.* **44**, 1150 (2019).
- Black, E. D. An introduction to Pound-Drever-Hall laser frequency stabilization. *Am. J. Phys.* **69**, 79 (2001).

42. Zhang, W. et al. Ultranarrow linewidth photonic-atomic laser. *Laser Photonics Rev.* **14**, 1900293 (2020).
43. Brasch, V., Lucas, E., Jost, J. D., Geiselmann, M. & Kippenberg, T. J. Self-referenced photonic chip soliton Kerr frequency comb. *Light* **6**, e16202 (2017).
44. Rao, A. et al. Towards integrated photonic interposers for processing octave-spanning microresonator frequency combs. *Light* **10**, 109 (2021).
45. Guo, J. et al. Chip-based laser with 1-hertz integrated linewidth. *Sci. Adv.* **8**, eabp9006 (2022).
46. Shao, L. et al. Integrated microwave acousto-optic frequency shifter on thin-film lithium niobate. *Opt. Express* **28**, 23728 (2020).
47. Hu, Y. et al. On-chip electro-optic frequency shifters and beam splitters. *Nature* **599**, 587 (2021).
48. Lu, J. et al. Periodically poled thin-film lithium niobate microring resonators with a second-harmonic generation efficiency of 250,000%/w. *Optica* **6**, 1455 (2019).
49. Li, M. et al. Integrated pockels laser. *Nat. Commun.* **13**, 5344 (2022).
50. Steck, D. A. Rubidium 87 d line data. <http://steck.us/alkalidata> (2001).

Acknowledgements

The work was supported by the National Natural Science Foundation of China (12293052, 11934012, 12104442, 92050109, 92250302, and 12304435), the Innovation Program for Quantum Science and Technology (2021ZD0303203), the CAS Project for Young Scientists in Basic Research (YSBR-069), the Fundamental Research Funds for the Central Universities and China Postdoctoral Science Foundation (2023M733414). This work was partially carried out at the USTC Center for Micro and Nanoscale Research and Fabrication.

Author contributions

R.N. and S.W. contribute equally to this work. R.N., S.W., and C.-H.D. conceived the experiments, S.W., P.Y. Wang, W.L., and F.B. prepared devices, R.N. and S.W. built the experimental setup and carried out measurements, and J.L. analyzed the data. R.N., S.W., and C.-H.D. wrote the paper with input from all co-authors. C.-H.D., F.-W.S., and G.-C.G. supervised the project. All authors contributed extensively to the work presented in this paper.

Competing interests

The authors declare no competing interests.

Additional information

Supplementary information The online version contains supplementary material available at <https://doi.org/10.1038/s42005-023-01452-1>.

Correspondence and requests for materials should be addressed to Fang Bo or Chun-Hua Dong.

Peer review information *Communications Physics* thanks Cheng Wang and the other, anonymous, reviewer(s) for their contribution to the peer review of this work. A peer review file is available.

Reprints and permission information is available at <http://www.nature.com/reprints>

Publisher's note Springer Nature remains neutral with regard to jurisdictional claims in published maps and institutional affiliations.



Open Access This article is licensed under a Creative Commons Attribution 4.0 International License, which permits use, sharing, adaptation, distribution and reproduction in any medium or format, as long as you give appropriate credit to the original author(s) and the source, provide a link to the Creative Commons licence, and indicate if changes were made. The images or other third party material in this article are included in the article's Creative Commons licence, unless indicated otherwise in a credit line to the material. If material is not included in the article's Creative Commons licence and your intended use is not permitted by statutory regulation or exceeds the permitted use, you will need to obtain permission directly from the copyright holder. To view a copy of this licence, visit <http://creativecommons.org/licenses/by/4.0/>.

© The Author(s) 2023